

ATMOSPHERIC PHASE DRIFT ANALYSIS AND COMPENSATION IN PERMANENT GB-SAR MONITORING OF CROP FIELDS

Héctor Palacio, Antoni Broquetas, Alberto Aguasca

CommSensLAB, Universitat Politècnica de Catalunya

ABSTRACT

In the framework of a feasibility study in support of the Hydroterra mission, a high resolution radar has been setup to monitor continuously a crop field with high resolution synthetic aperture radar images. In parallel, ground-truth data is acquired such as soil roughness, soil moisture and crop biological parameters. From this experimental data set the possibility to monitor soil moisture and crop biological parameters from back-scattering radar measurements will be assessed. To use the phase information of SAR images it is interesting to compensate the atmospheric phase screen induced by tropospheric refractive index. The paper presents a study of the atmospheric phase drift prediction and compensation based on the local measurement of meteorological parameters.

Index Terms— GB-SAR, Phase Drifts, Calibrator

1. INTRODUCTION

The European Space Agency (ESA) is currently in Phase 0 study of the Hydroterra Geosynchronous Radar Satellite Mission[1]. This mission will offer a continuous Synthetic Aperture Radar (SAR) monitoring of the Earth. To study the agricultural applications of Hydroterra, the Universitat Politècnica de Catalunya has set up a Ground-Based SAR (GB-SAR) system, monitoring an agricultural field of the Barcelona School of Agri-food and Biosystems Engineering (EEABB). The radar operates with a linear positioner on top of the EEABB building offering excellent stability. After the appropriate SAR processing, the system provides high-resolution images of the field. In order to study the parameters of the amplitude and phase of the SAR images, the troposphere plays an important part. The temperature, the humidity and air pressure are three of the most important factors to take into account when looking at the results obtained by the continuous radar. The aim of this research paper is to study the relationship between the amplitude and the phase of the SAR images and these three factors, in order to compensate the error of the troposphere from the final images.

1.1. System Overview

The radar is located at the top of the 20 meters height EEABB building resulting in an incidence angle over the test field from 50° to 67° , very similar to the ones that the Hydroterra mission plans to have when observing the South of Europe. The test field is rectangular with a size of 22 m in range and 60 m in azimuth. Two crops have been monitored so far, first a cereal, barley (*hordeum vulgare*) from March to June 2020. After harvesting barley and installing an irrigation system corn was sown at the end of June and harvested in November. In Figure 1, the overview of the radar and its incidence on the rectangular field can be seen.



Fig. 1. Overview of the system at EEABB-UPC in May 2019

1.2. Basic Radar Parameters

The radar instrument is a Linear FM-CW homodyne system based on Direct Digital Synthesizer (DDS), configured as Ground Based SAR (GB-SAR)[2]. The synthetic aperture of the radar is 1.5 m. The radar is using a carrier frequency of 5.6 GHz (C-Band) with a 200 MHz Bandwidth. In this way a metric spatial resolution is obtained in both range and cross-range axes of the SAR images.

The Radar observes the test field in a continuous monitoring mode delivering polarimetric data acquisitions every 10 minutes from March 2020 with the exception of two short maintenance stops.

2. IMPLEMENTATION

2.1. Selection of an appropriate time

The first step was to identify an appropriate time interval in which the crop fields at EEABB experimented a big change both in humidity and temperature. A meteorological station located at 25 m from the EEABB test field was used in order to obtain the meteorological data needed. The station data contained information of the temperature, humidity and pressure every 10 minutes from May to September. Although any change of these parameters in a short time range would be noticed in the phase and amplitude images, a fast and large change event was selected in order to facilitate the study.

An interesting meteorological parameters change was found from 23h to 06:40h during the night of the 2nd of August in 2020. During this almost 7 hours (resulting in 47 acquisitions every 10 minutes), the humidity changed from approximately 84% to 50% within 3 hours and then back again to 80% in 2 hours. During these hours a big change in the temperature was experimented as well, as the temperature dropped from 27 degrees to 18 degrees (Celsius). A big change in temperature was specially seen for 30 minutes from 5:20h to 5:50h, as the temperature drop during that time range was very significant. The temperature and humidity evolution throughout that time slot are represented in Figure 2 and will be further analysed and compared in the following sections.

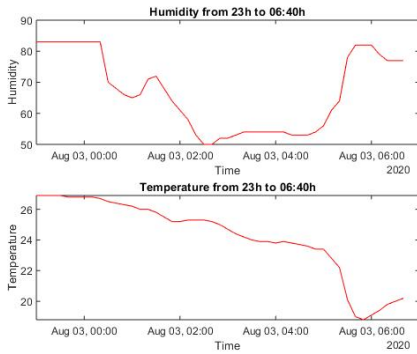


Fig. 2. Humidity and Temperature evolution from 23h to 06:40h

2.2. Calculation of the atmospheric refractive index

In order to compute the refractive index, the ITU-R P.453-11 (07/2015)[3] standard has been used.

This standard calculates the radio refractive index (n) depending on different parameters. The refractive index is obtained through the previous calculation of the radio refractivity (N). This value is obtained using the following equation of the standard:

$$N = 77.6 \cdot \frac{Pd}{T} + 72 \cdot \frac{e}{T} + 3.75 \cdot 10^5 \cdot \frac{e}{T^2} \quad (1)$$

where Pd is the dry atmospheric pressure (hPa), e is the water vapour pressure (hPa) and T is the absolute temperature (K). The water vapour pressure e is a parameter that directly depends on the humidity values, and can be computed by following this equation:

$$e = \frac{H}{100} \cdot EF \cdot a \cdot \exp\left[\frac{b - \frac{t}{d}}{t + c}\right] \quad (2)$$

where

$$EF = 1 + 10^{-4} \cdot [7.2 + P \cdot (0.0032 + 5.9 \cdot 10^{-7} \cdot t^2)] \quad (3)$$

and $a = 6.1121$, $b = 18.678$, $c = 257.14$, $d = 234.5$. As for the rest of the variables, t is the temperature in Celsius and H the relative humidity in %.

Once the radio refractivity N is computed, the final step is to compute the radio refractive index based on the atmospheric parameters following the simple equation:

$$n = 1 + N \cdot 10^{-6} \quad (4)$$

In this way, a computation of the refractive index every 10 minutes -that is, 47 values- during the acquisition time chosen (23h to 06:40h) has been done and can be seen in Figure 3.

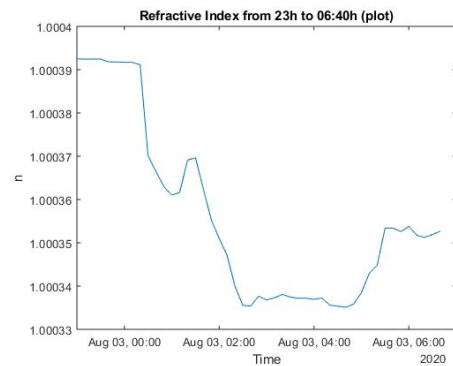


Fig. 3. Atmospheric refractive index evolution from 23h to 06:40h

The refractive index parameter is extremely correlated to the humidity values shown in Figure 2, with a lighter increase of the refractivity in the final hours of the acquisition period, due to the sudden increase of temperature. The value of the refractive index experiences a maximum difference in value of 0.00006 implying a phase shift of about one radian at a radar range of 80 m.

2.3. Amplitude and Phase changes retrieval

Once the values of the refractive index are calculated, they can be used in order to theoretically obtain the phase changes of the SAR images in the acquisition day chosen for this study.

The acquired radar raw-data every 10 minutes is processed with a Back-Projection algorithm in order to focus on the sequence of images of the area of interest. To measure the changes in amplitude and phase of the radar images, three corner-reflector calibrators have been physically set up in the EEABB Test Field at different distances and with different polarimetric signatures. The calibrators are located at 36 m, 60 m and 80 m in range, and 0° , 20° and -12° azimuth respectively. The first one and the last one are co-polar targets providing a peak in the VV and HH polarizations, while the second calibrator -a 45 degree tilted dihedral- is a cross-polar calibrator appearing in the VH and HV images.

The processing of all 47 images consists in selecting one of the three calibrators with the appropriate polarization and a comparison is done between the amplitude and phase values of the master image (the first one at 23h) and the rest of them. The first value of both amplitude and phase is saved and a difference is computed between the 46 slave remaining images and the master one.

This difference is computed, as it has been said, in the maximum reflection pixel of the image for each calibrator and its polarization, so there are a total of 6 results (3 for the amplitude and 3 for the phase). These results will be the so-called on-the-ground results, that will be later on compared to the phase theoretical ones using the refractive index values obtained in the previous section, as the refractive index values **only** affect the phase and not the amplitude.

The theoretical results of the phase change values in the calibrators are obtained through the following equation:

$$\Delta\phi = \phi_{master} - \phi_{slave} \quad (5)$$

where

$$\phi_i = -2 \cdot 2 \cdot \pi \cdot f_0 \cdot \frac{d}{n_i} \quad (6)$$

where f_0 is the central frequency (5.6 GHz), d is the distance to the maximum reflection pixel (being 36, 60 or 80 m), c is the light velocity in vacuum and n is the refractive index in each image.

2.4. Analysis of the results (theoretical vs experimental)

The final step of this study is to analyse the difference between the theoretical phase change expected from the meteorological data of the station (at 25 m from the crop field) and the on-the-ground values obtained. A study on the changes of the amplitude will be made as well in order to see the correlation with other meteorological parameters.

Figure 4 shows the three different plots regarding the theoretical phase differences between the slaves images and the master one. As it can be seen, by following the equation (6) shown earlier this document, the closer is the calibrator, the less phase difference appears between each acquisition image. In the 80 m range calibrator, the changes in the phase are more significant as there is more distance to be covered by the signal, resulting in almost 1 rad of difference in some images with respect to the master one.

All three plots have a very strong correlation with the refractive index, that has a strong correlation to the humidity as well. It can be concluded that a very strong relationship between the humidity and the phase changes in the radar echoes exists. The temperature does not show any type of significant correlation with the phase.

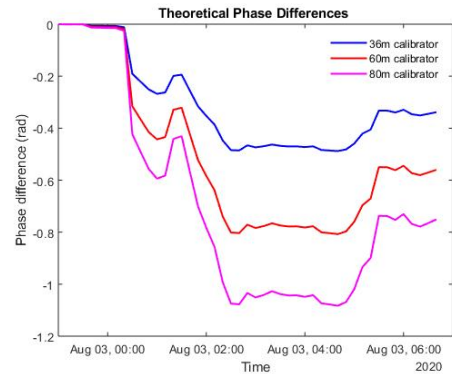


Fig. 4. Theoretical Phase Difference from 23h to 06:40h

Moving on from the theoretical plots to the experimental ones obtained, the results are as expected. The span of the phase shift obtained from the measurements is very similar to the theoretical prediction. However, there are some differences between the plots. Specifically, in the acquisition times from 5:20h to 5:40h (a total of 3 acquisitions) the experimental phase shift is notably larger compared to the theoretical plot which cor-

responds to a fast humidity/temperature change. This discrepancy may be caused by the fact that the air humidity/temperature parameters measured by the meteorological station 25 m away from the field may have not reproduced exactly the air parameters over the field with a corn crop growing in an irrigated soil.

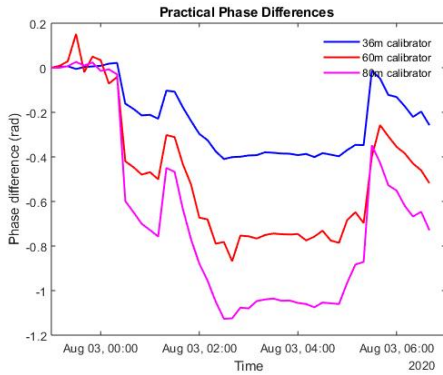


Fig. 5. Practical Phase Difference from 23h to 06:40h

Finally, there is an extra study that has been made regarding the amplitude difference in the maximum reflection values of the calibrators. In Figure 6, the three overlapped plots of the calibrators are a lot different than the phase plots, and that is because they do not hold a strong correlation with the humidity but with the **temperature**, probably due to the thermal gain drift of the radar electronics. This can be easily seen by comparing them with Figure 2. However, the order of the plots is reversed from the last two Figures. The 36 m calibrator is the one that is more affected by the temperature decrease at around 5:20am, while the other two calibrators show a less abrupt change at that specific time.

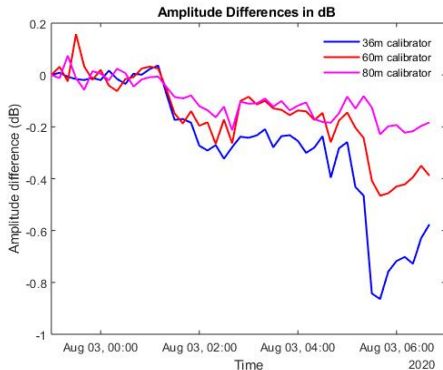


Fig. 6. Amplitude Difference in dB from 23h to 06:40h

3. CONCLUSION AND FURTHER WORK

The results of this research paper conclude that there is a strong correlation between the phase changes in the continuous GB-SAR echoes and the refractive index evolution and that the temperature severely affects the amplitude images of the SAR. The difference between the theoretical and experimental results will always be present due to the fact that the meteorological data comes from a station located at 25 m from the Test Field rather than *in situ* meteorological data acquisitions.

The next step would be to compute the differential error produced by the troposphere effects taking advantage of the measurements in the three calibrators and use them to cancel the residual error in the SAR acquisitions. The accuracy of all the images would increase dramatically and their results would be more enlightening to further tests for the ESA Hydroterra mission. The ideal method would be to compute different weight values depending on parameters such as temperature, humidity or distance of the calibrator in order to automatically cancel the atmospheric error.

Another possible future study to be considered would be to make an extensive amplitude analysis on the three different calibrators located in the crop field. More insights on this should be studied in further research in order to better understand the way the thermal gains of the continuous GB-SAR components affect the amplitude of the images.

4. REFERENCES

- [1] SE Hobbs and A Monti-Guarnieri. Geosynchronous continental land-atmosphere sensing system (g-class): persistent radar imaging for earth science. In *IGARSS 2018 - IEEE International Geoscience and Remote Sensing Symposium*, July 2018.
- [2] A. Aguasca, A. Broquetas, J. J. Mallorqui, and X. Fabregas. A solid state l to x-band flexible ground-based sar system for continuous monitoring applications. In *IGARSS 2004. 2004 IEEE International Geoscience and Remote Sensing Symposium*, volume 2, pages 757–760, 2004.
- [3] The radio refractive index: its formula and refractivity data. ITU-R P.453-11(07/2015) . Standard, International Telecommunication Union, July 2015.